Check for updates

Received: 12 June 2023 | Revised: 22 August 2023 | Accepted: 28 August 2023

DOI: 10.1111/micc.12830

Microcirculation WILEY

ORIGINAL ARTICLE

Estimation of shear stress heterogeneity along capillary segments in angiogenic rat mesenteric microvascular networks

Nien-Wen Hu[1] | Banks M. Lomel[1] | Elijah W. Rice[1] | Mir Md Nasim Hossain[2] | Malisa Sarntinoranont[3] | Timothy W. Secomb[4] | Walter L. Murfee[1] | Peter Balogh[2]

[1]J. Crayton Pruitt Family Department of Biomedical Engineering, University of Florida, Florida, Gainesville, USA

[2]Department of Mechanical and Industrial Engineering, New Jersey Institute of Technology, New Jersey, Newark, USA

[3]Department of Mechanical and Aerospace Engineering, University of Florida, Florida, Gainesville, USA

[4]Department of Physiology, University of Arizona, Arizona, Tucson, USA

Correspondence
Peter Balogh, Department of Mechanical and Industrial Engineering, New Jersey Institute of Technology, 324A Mechanical Engineering Center, University Heights, Newark, NJ 07102, USA.
Email: peter.balogh@njit.edu

Funding information
Cancer Center, University of Florida Health, Grant/Award Number: 00096885 CA-FY22-03; National Institutes of Health, Grant/Award Number: R21HL159501

Abstract

Objective: Fluid shear stress is thought to be a regulator of endothelial cell behavior during angiogenesis. The link, however, requires an understanding of stress values at the capillary level in angiogenic microvascular networks. Critical questions remain. What are the stresses? Do capillaries experience similar stress magnitudes? Can variations explain vessel-specific behavior? The objective of this study was to estimate segment-specific shear stresses in angiogenic networks.

Methods: Images of angiogenic networks characterized by increased vascular density were obtained from rat mesenteric tissues stimulated by compound 48/80-induced mast cell degranulation. Vessels were identified by perfusion of a 40 kDa fixable dextran prior to harvesting and immunolabeling for PECAM. Using a network flow-based segment model with physiologically relevant parameters, stresses were computed per vessel for regions across multiple networks.

Results: Stresses ranged from 0.003 to 2328.1 dyne/cm^2 and varied dramatically at the capillary level. For all regions, the maximum segmental shear stresses were for capillary segments. Stresses along proximal capillaries branching from arteriole inlets were increased compared to stresses along capillaries in more distal regions.

Conclusions: The results highlight the variability of shear stresses along angiogenic capillaries and motivate new discussions on how endothelial cells may respond in vivo to segment-specific microenvironment during angiogenesis.

KEYWORDS
angiogenesis, computational fluid dynamics, endothelial cell, microvascular network, shear stress

1 | INTRODUCTION

Shear stress is commonly implicated in angiogenesis, defined as the formation of new blood vessels from existing vessels. The role of shear stress as a regulator of endothelial cell dynamics during capillary sprouting is supported by the influences on cell phenotype, proliferation, and function.[1,2] As altered angiogenesis is associated with multiple pathologies like diabetes, cancer, and myocardial infarction, understanding how shear stress might influence endothelial cell dynamics is important and could provide insight into what goes wrong in disease scenarios. In vitro experiments have suggested that shear stress triggers sprouting,[3] cell proliferation,[4] tube formation,[5] cell migration,[6] and growth factor expression,[7] and regulates vessel density,[8] permeability,[9] cell phenotype,[10] and matrix production.[11] However, consideration of the literature provokes questions about the appropriate shear stress range and what values are actually experienced by endothelial cells in real angiogenic microvascular networks. Galie et al. used a microfluidic device to show that both

 © 2023 John Wiley & Sons Ltd.

luminal and transmural shear stress of 10–30 dyne/cm^2 induce endothelial cell sprouting.[3] Song et al. showed using a similar microfluidic device that 3 dyne/cm^2 mitigates endothelial cell migration, invasion, and proliferation.[12] Compare these results to a study by Kang et al., which showed that shear stress of 3–5.3 dyne/cm^2 stimulated sprout formation by cells cultured in three dimensions and that 12 dyne/cm^2 inhibited growth.[13] Shear stress values used to study endothelial cell responses range from 0.1 to 50 dyne/cm^2.[14–16] Even studies using 100 dyne/cm^2[17] can be found. The range in shear stresses used for in vitro studies and the variable responses provoke additional questions about the physiological relevance of the assays. A confounding issue is that it is difficult to measure shear stress or vessel-specific velocity gradients across angiogenic vessels during active network remodeling. While the role of shear stress is also supported by in vivo studies,[2] the actual shear stress values experienced by endothelial cells along angiogenic capillaries are understudied.

Computational modeling offers a valuable approach to appreciate potential shear stress values in microvascular networks. In a few examples from the literature, computational studies have estimated stresses in networks, although these have primarily focused on unstimulated or non-angiogenic networks. For example, Ganesan et al. modeled blood flow and shear stress distribution in mouse retina networks,[18] and their results suggest that shear stresses along distal capillaries can range from 0.1 to 300 dyne/cm^2. In several studies, Pries et al.[19–24] used a network flow model to predict distributions of hematocrit, pressure, flow velocity, and shear stress in rat mesenteric networks to investigate vascular network resistance, vascular pressure-shear stress homeostasis, and adaptive vascular remodeling and regression. Their collective studies in non-angiogenic networks suggest that segment-specific shear stress along capillaries can range from 0.1 to 500 dyne/cm^2. Using a three-dimensional network flow model, Balogh et al. simulated RBC and plasma flow in idealized rat spinotrapezius muscle capillary networks to evaluate and report shear stress (5–50 dyne/cm^2) and its gradient distribution (0.1–12 [dyne/cm^2]/μm) across the microvascular networks, among vessel types, and at bifurcations and mergers.[25]

Computational studies investigating wall shear stress values that can occur in angiogenic microvascular networks are extremely rare. Bernabeu et al.[26] reported shear stress values in developing retinal networks up to 200 dyne/cm^2, although the predicted distribution of average per-vessel shear stress values versus diameter across the networks was unclear. Work by Ghaffari et al. reported shear stress values in isolated microvascular loop structures of avian chick embryos,[27] with values around the loops reaching as high as a 1.4 dyne/cm^2. Such information in angiogenic vessels has, importantly, provided some examples of values that can occur, but full shear stress distributions across angiogenic networks, similar to those provided by studies in unstimulated or non-angiogenic networks, do not exist to our knowledge. This marks a major gap in current understanding because angiogenic networks have distinctly different network structures and characteristics than non-angiogenic networks. Based on fluid mechanical considerations, one might thus expect different wall shear stress characteristics to exist, yet such direct comparisons are also lacking. Based on these considerations, knowledge of shear stress distributions unique to angiogenesis can provide a needed characterization of this important quantity known to influence endothelial cell responses.

The variable shear stress values associated with in vitro studies, the understudied in vivo values, and the scarcity of computational models focused on angiogenic networks motivate the current study. What is the shear stress that endothelial cells in capillaries experience during angiogenesis? Are the shear stress magnitudes experienced by all capillaries similar? Could the segment-specific endothelial responses be dependent on variations in shear stress among capillaries? The objective of this study was to estimate segment-specific shear stresses in angiogenic networks and provide context by also comparing them with shear stresses in non-angiogenic networks in the same type of tissue.

Using geometric measurements in angiogenic networks from rat mesenteric tissues stimulated by compound 48/80-induced mast cell degranulation[28] and physiologically relevant pressures, shear stress values were estimated per segment using a network flow-based model. Our results suggest that shear stresses are heterogeneous and can vary by orders of magnitude. The dramatic heterogeneity is further supported by complementary initial three-dimensional computational modeling and the incorporation of local RBC effects. Altogether, our findings should motivate new discussions among vascular biologists on the potential effects of shear stress during angiogenesis in vivo, and, in particular, the importance of spatial and temporal shear stress distributions associated with microvascular remodeling.

2 | MATERIALS AND METHODS

2.1 | Angiogenic microvascular network analysis

Network images were obtained by re-imaging of angiogenic adult rat mesenteric tissues from a previous study.[28] As described in the study by Sweat et al., angiogenesis was stimulated via i.p. injections of compound 48/80, a mast cell degranulator. Post-stimulation, perfusion of fixable 40 kDa FITC-dextran identified vessel lumens. Vessel segments were additionally confirmed by the labeling of endothelial cells for PECAM (Figure 1). Mesenteric tissues were whole mounted and observed en face. The mesentery's thinness (20–40 μm) enables imaging of intact networks at the vessel and cellular levels and eliminates the need for tissue sectioning. Angiogenic microvascular networks were characterized by increased segment density and sprouting[28] compared to unstimulated microvascular networks. Representative microvascular network regions with arteriolar inlet(s), venular outlet(s), and arteriolar-venular loop(s) were selected and captured using 4x (dry, NA = 0.1) and 10x (dry, NA = 0.3) objectives on an inverted microscope (Nikon Ti2) coupled with an ANDOR Zyla sCMOS camera, as shown in Figure 1: (1) One large region with 3200 segments (Figure 1a), (2) three medium regions with 150 to 450 segments (Figure 1b), and (3) four small regions with 50

15498719, 2023, 8, Downloaded from https://onlinelibrary.wiley.com/doi/10.1111/micc.12830 by Nj Institute Of Technology, Wiley Online Library on [03/06/2024]. See the Terms and Conditions (https://onlinelibrary.wiley.com/terms-and-conditions) on Wiley Online Library for rules of use; OA articles are governed by the applicable Creative Commons License

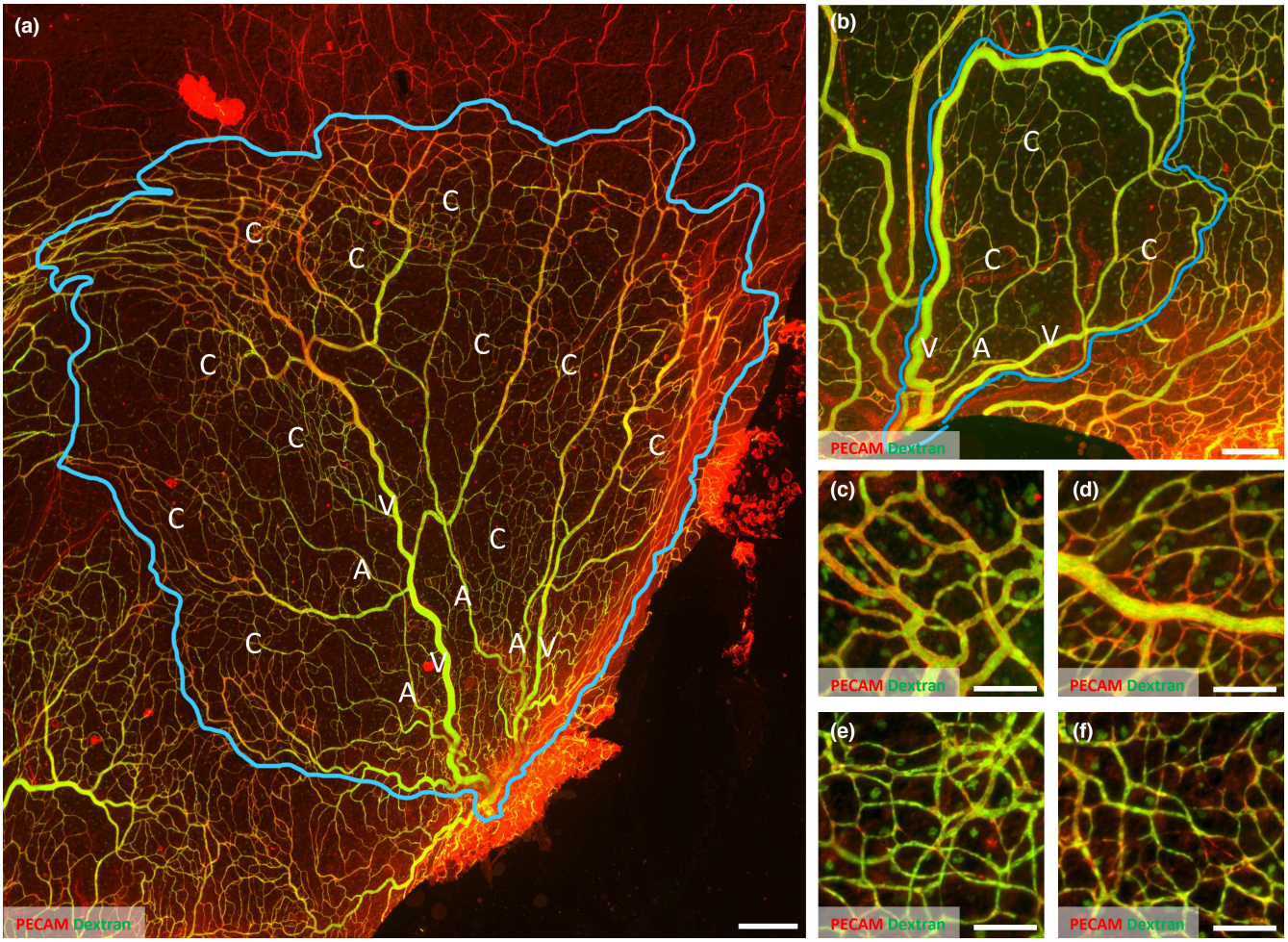

FIGURE 1 Representative images of angiogenic rat mesentery tissues with clearly identifiable vascular networks. Mesentery tissues were harvested from adult Wistar rats treated with 48/80 to induce mast cell degranulation and angiogenesis. Prior to tissue harvesting, networks were perfused with a fixable 40 kDa Dextran (Green) to show vessel patency. Post-harvesting, tissues were labeled for PECAM (Red). (a) & (b) Vascular networks with were selected based on identifiable arteriole inlet(s) (labeled with A), venule outlet(s) (labeled with V), capillaries (labeled with C), and arteriole-capillary-venule loops. (c–f) Additional smaller vascular regions for evaluation of stress distributions associated with different high density capillary patterns. The blue line marked the selected vascular network regions for computational modeling. Scale bar: (a) 400 μm (b) 200 μm (c–f) 100 μm.

to 150 segments (Figure 1c–f). The rationale for region selection is supported by the overall goal of the study to appreciate potential shear stress values across different vessel types and representative network patterns associated with angiogenic remodeling. The smaller regions enabled the evaluation of stress distributions associated with different high-density capillary patterns. A vessel segment was defined as a segment between two nodes, which were the branch points where more than two segments intersected. The measurements of lengths and diameters were facilitated from the images based on the centerline distance per segment and the average perpendicular distance between vessel walls defined by the dextran labeling.

The measurements of lengths and diameters were facilitated from the images based on the centerline distance per segment and the average perpendicular distance between vessel walls defined by the dextran labeling. Specifically, for image-based measurements, a microscopic image was opened in Image J set with the correct scale ratio according to the magnification of the image (4×: 0.613 pxl/μm, 10×: 1.538 pxl/μm). The diameter of each segment was recorded using the ROI manager. Medium regions were zoomed in three times, and the large regions were zoomed in five times. Each segment was then visually inspected, and the diameter was measured as the line distance perpendicular to the wall over a cross-section that best represented the vessel. Each measurement was added to the ROI manager. In total, eight regions were analyzed from three tissues. We note that for the medium regions presented later in Figure 5, any apparent differences in diameters between the two color maps for each respective network are likely due to visual artifacts arising from the same vessels being represented by different colors. In order to evaluate the estimated shear stress in vascular networks on angiogenic tissues, a comparison was made using a two-tailed Student's *t*-test between two experimental groups: unstimulated (control) and stimulated tissues. Results were considered statistically significant when $p \leq .05$. Values are presented as mean ± standard error of the mean (SEM).

15498719, 2023, 8, Downloaded from https://onlinelibrary.wiley.com/doi/10.1111/micc.12830 by Nj Institute Of Technology, Wiley Online Library on [03/06/2024]. See the Terms and Conditions (https://onlinelibrary.wiley.com/terms-and-conditions) on Wiley Online Library for rules of use; OA articles are governed by the applicable Creative Commons License

2.2 | Network segment model overview

As shown in Figure 2, a network segmental flow model was used to computationally estimate segment-specific shear stresses, similar to previous studies.[23,29] Input geometry data included the adjacent nodes (branch points), diameters, lengths, and branch orders of vascular segments. Blood flow was determined per segment following the Poiseuille flow relationship for two cases: constant viscosity (μ = 4 cP) and changing segmental viscosities based on an empirical relationship previously established for the rat mesenteric microcirculation.[22] For the changing viscosity cases, the apparent viscosity of blood in vessel segments was initially set to be 4 cP and then updated based on the empirical relationship, which is dependent on segment diameters, segmental hematocrit, and velocity.[29] The hematocrit for all segments was initially set to be 0.45. Based on the empirical equations, segment-specific hematocrits were calculated with the diameters of daughter segments, the hematocrits and segmental flow of daughter and parent segments, and the fraction of red blood cell flow. The updated hematocrits were then used to calculate segment-specific viscosity (μ). With the updated segmental viscosity, the nodal pressures and flow rates were recalculated using Equation 2 in an iterative fashion. The segmental shear stresses were also updated. For both cases, Equation 1 was used to calculate the conductance of each segment[29]:

$$C = \frac{\pi D^4}{128\,\mu L} \tag{1}$$

The pressures of the arteriolar inlet(s) and venular outlet(s) were set to be 75 and 10 mm Hg. For the smaller microvascular regions shown in Figure 1c–f, which had many inlets and outlets, the pressures were assigned based on a previously reported pressure-diameter correlation.[20] With assigned pressures (P) and segmental conductances (C), the nodal flow rates (Q) and other nodal pressures can be calculated by using the matrix equation derived from the conservation of mass (Equation 2):

$$\boldsymbol{Q = CP} \tag{2}$$

To be more specific, the nodal flow rates and pressures were calculated from the first node to the last node, updating new values into the matrices. Using the updated matrices, the nodal flow rates and pressures can be recalculated since the matrices have more values. Following this logic, the model was designed to check the segmental pressure difference between the updated pressure matrix and the previous iteration. The threshold for the loop iteration to stop was meeting the conversion requirement, defined as a total segmental pressure difference less than 10^{-3} mm Hg. With the updated nodal pressure and flow rates, the segmental shear stresses (τ) can be calculated by using the following equation (Equation 3):

$$\tau = \left|\frac{D \bullet \Delta P}{4\,L}\right| \tag{3}$$

For the changing viscosity cases, the apparent viscosity of blood in vessel segments was initially set to be 4 cP and then updated based on the empirical relationship, which is dependent on segment diameters, segmental hematocrit, and velocity as per the following in vivo viscosity law from Pries et al.[19]:

$$\mu_c = \left\{1 + (\mu^* - 1)\frac{(1-H_D)^\alpha - 1}{(1-0.45)^\alpha - 1}\left(\frac{D}{D-1.1}\right)^2\right\}\left(\frac{D}{D-1.1}\right)^2 \tag{4}$$

where estimated viscosity (μ^*), hematocrit (H_D) and α were calculated based on equations described elsewhere.[19] Further, the calculation of H_D in each segment incorporates a phase separation model also described elsewhere,[30] to account for the non-uniform partitioning of RBCs at bifurcations. The hematocrit for all segments was initially set to be 0.45. The segment-specific hematocrits (μ_c) were calculated with the diameters of daughter segments, the hematocrits and segmental flow of daughter and parent segments, and the fraction of red blood cell flow. The updated hematocrits were then used to calculate segment-specific viscosity (μ). With the updated segmental viscosity, the nodal pressures and flow rates were recalculated using Equation 2 in an iterative fashion. The segmental shear stresses were also updated.

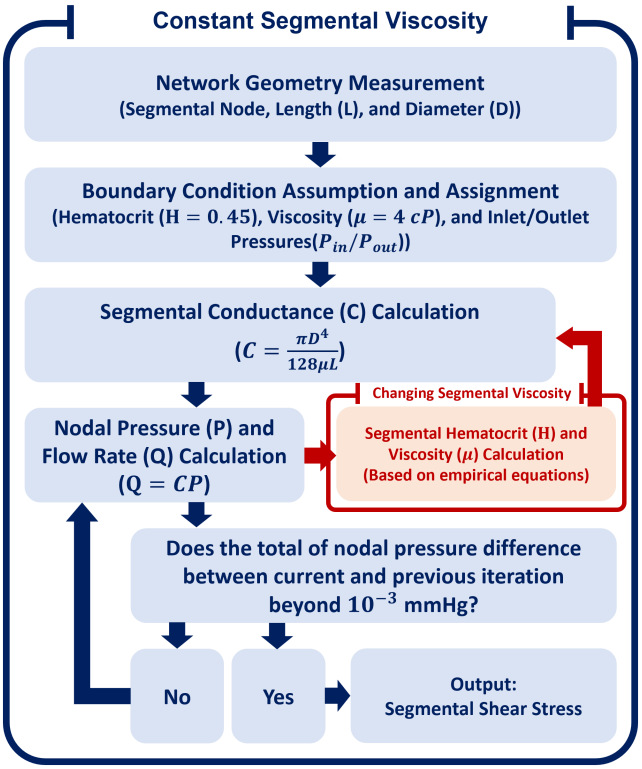

FIGURE 2 Overview of modeling approach used to simulate vascular network. The computational model was simulating network flow with physiologically relevant geometric data (adjacent nodes, lengths, and diameters of vascular segments) measured from real rat mesentery tissues. The inlet and outlet pressures were set to be 75 and 10 mm Hg. By assuming a constant plasma viscosity of 4 cP or computed segment-specific viscosity, the segment conductance, nodal pressure, and flow as well as shear stress were further calculated by using the equations a loop iteration.

15498719, 2023, 8, Downloaded from https://onlinelibrary.wiley.com/doi/10.1111/micc.12830 by Nj Institute Of Technology, Wiley Online Library on [03/06/2024]. See the Terms and Conditions (https://onlinelibrary.wiley.com/terms-and-conditions) on Wiley Online Library for rules of use; OA articles are governed by the applicable Creative Commons License

2.3 | Three-dimensional model overview

The rationale for using the network modeling approach is supported by its previous use in the literature to estimate segmental hemodynamics in large microvascular networks. However, limitations of this approach include the lack of red blood cells (RBCs) and not including three-dimensional vessel shapes (i.e., tortuosity, segment paths). In order to evaluate the potential impact of these limitations and the assumptions related to the viscosity cases, additional three-dimensional RBC-resolved simulations were performed. While such simulations provide higher-resolution output, they require a significant increase in computational cost. Given that the focus of the current work is on the estimation of segmental shear stresses and heterogeneity, the application of the 3D model is limited here to a small angiogenic network region. The purpose is to provide a generalized corroboration of findings using the network model as discussed later, and the analysis is simply meant to highlight the potential for additional angiogenic heterogeneity.

RBC-resolved simulations were performed using an immersed boundary method (IBM)-based 3D fluid dynamics solver for modeling flows in complex geometries.[31] With this approach, an RBC is modeled as a 3D sac of viscous fluid enclosed by a zero-thickness elastic membrane. The initial undeformed RBC shape is taken as a biconcave disc. The membrane is represented by a Langrangian mesh of triangular elements that deforms as it flows with the fluid (plasma) in which the cell is immersed. RBC deformation is two-way coupled to the surrounding fluid using a continuous forcing-type IBM, where a delta function connects a cell mechanics model solved on the Lagrangian mesh to a fluid dynamics solver on a fixed Eulerian mesh. The membrane stresses in response to cell deformation are calculated using the finite element method, with loop elements used as a subdivision surface for the force calculations. The membrane model accounts for elasticity[32] as well as bending resistance, which are controlled through the membrane shear elastic modulus (G_s) and bending modulus (E_b), respectively. Here we use $G_s = 5 \times 10^{-6}$ N / m and $E_b = 2 \times 10^{-19}$ J, which correspond to values for healthy RBCs.[32,33]

The governing fluid flow equations are the Navier–Stokes equations for a constant density (ρ) variable viscosity (μ) fluid:

$$\rho \frac{D\boldsymbol{u}}{dt} = -\nabla P + \nabla \cdot \left[\mu\left(\nabla \boldsymbol{u} + \nabla \boldsymbol{u}^T\right)\right] + \boldsymbol{F} \quad (5)$$

These equations are solved for the fluid velocity ($\boldsymbol{u}$) and pressure (P) on the fixed Eulerian mesh with a projection method using a finite volume/spectral approach, where the body force term $\boldsymbol{F}$ incorporates stresses from the deformable cell model. Complex vascular walls are modeled with a sharp-interface ghost node IBM, which decomposes the Eulerian computational domain into a fluid domain inside the vessels and a solid domain outside. The interface conditions at the walls are enforced when solving Equation 5 via contains imposed at the Eulerian mesh points immediately outside the fluid domain. Wall shear stress is calculated following the approach outlined in our previous work.[25]

3 | RESULTS

3.1 | Shear stress magnitudes show high heterogeneity at the capillary level and depend on location within a network

To evaluate vessel-specific average shear stress values at the capillary level in angiogenic networks, three representative microvascular regions were selected. The networks contained 150 to 450 segments, arteriolar inlets, venular outlets, and an arteriolar-venular loop (Figure 3a–c). Shear stresses along vascular segments in three microvascular regions denoted as "medium regions" for this study ranged from 0.1 to 1114.3 dyne/cm^2 (average = 81.3 ± 3.5 dyne/cm^2; Figure 3d). We note the potential for this average value among all vessels to be altered by different weightings (e.g., vessel length, area, etc.). However, the focus of this work is on the distribution or range of values, and thus this average value is just provided as a point of reference when considering the range. Increased segmental heterogeneity was more pronounced at the capillary level (vessels less than 10 μm) versus along vessels with larger diameters. The visualization of a shear stress color map per region for which values were binned from 0 to greater than 50 dyne/cm^2 emphasizes the vessel-specific heterogeneity within the same network (Figure 3e). In addition, the shear stresses experienced show systematic variations with the location of capillaries in the network (i.e., capillaries branching off the higher pressure arteriole inlets versus more distal capillaries closer to the venule side of a network). The average and maximum shear stress values in capillaries more proximal to the arteriolar inlets were significantly higher than those distal to both inlets and outlets (Figure 3f).

Potential limitations of our modeling approach are assumptions about inlet/outlet pressures and constant viscosity. In order to evaluate the influence of pressure values imposed as boundary conditions, an additional sensitivity analysis was conducted (Figure 5a). The inlet pressure was changed to consider three total pressure drop cases: 95 mmHg, 65 mmHg, and 35 mmHg. While the nominal values do change, the order of magnitude range in shear stress distribution was found to be independent of pressure drop assumptions. This result makes sense, as shear stress values changed linearly, increasing or decreasing with the same distribution pattern (Figure 4). The linear relationship is represented by the equation used to calculate shear stress in the model ($\tau = \left|\frac{D \cdot \Delta P}{4L}\right|$). Regarding the viscosity assumptions, we compared the constant viscosity simulation results to the case that simulated blood flow as non-Newtonian flow with viscosities and hematocrits dependent on the segment geometry and network hemodynamics (Figure 4B). The trend and distribution pattern were similar between the two assumptions.

The identification of heterogeneous shear stress distribution in the angiogenic network regions and, moreover, the suggestion of order of magnitude differences for capillaries within a network motivated additional studies to determine whether the heterogeneity was characteristic of different capillary plexus regions. Four local microvascular regions with 60 to 150 segments were selected for

15498719, 2023, 8, Downloaded from https://onlinelibrary.wiley.com/doi/10.1111/micc.12830 by Nj Institute Of Technology, Wiley Online Library on [03/06/2024]. See the Terms and Conditions (https://onlinelibrary.wiley.com/terms-and-conditions) on Wiley Online Library for rules of use; OA articles are governed by the applicable Creative Commons License

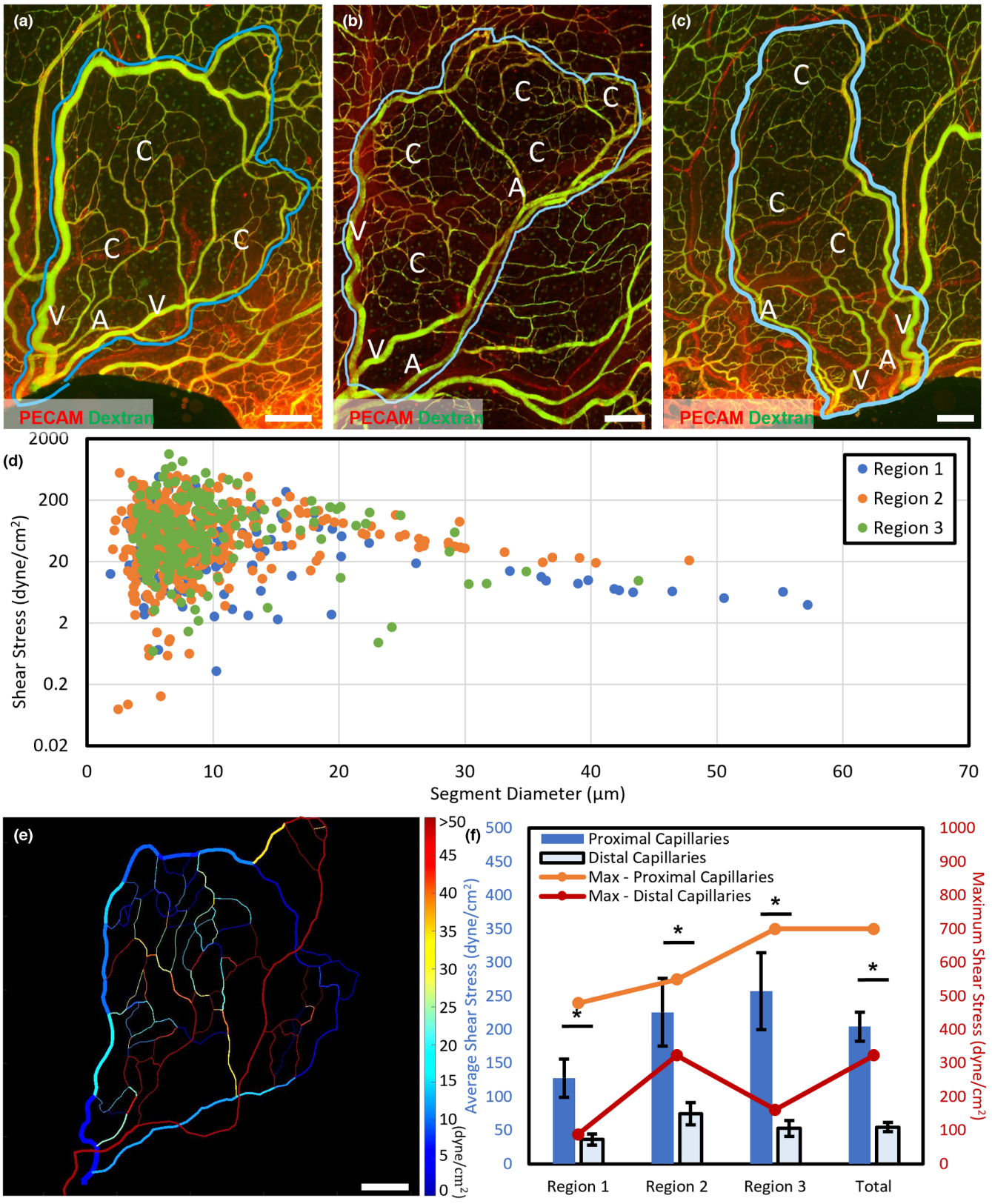

FIGURE 3 Shear stress estimates for single vascular segments in three vascular regions. (a–c) Network regions used for simulations. Vessel walls labeled with PECAM were shown in red and vessels perfused with 40 kDa Dextran were shown in green. (d) Distribution of shear stress values per segment diameter. Stress values in small segments (diameter: <10 μm) range from 0.1 to 1114 dyne/cm^2. with the standard deviation of 103 dyne/cm^2. (e) Color map of shear stress spatial distribution. Range = 0 (blue) to >50 (red) dyne/cm^2. (f) Comparisons across capillary segments proximal and distal to arteriolar inlet vessel. Labels: A, arteriole, V, venule, C, capillaries. The blue line marks the selected vascular network regions for computational modeling. Scale bar: (a–c) & (e) 200 μm. The asterisk indicates a p-value less than 0.05.

15498719, 2023, 8, Downloaded from https://onlinelibrary.wiley.com/doi/10.1111/micc.12830 by Nj Institute Of Technology, Wiley Online Library on [03/06/2024]. See the Terms and Conditions (https://onlinelibrary.wiley.com/terms-and-conditions) on Wiley Online Library for rules of use; OA articles are governed by the applicable Creative Commons License

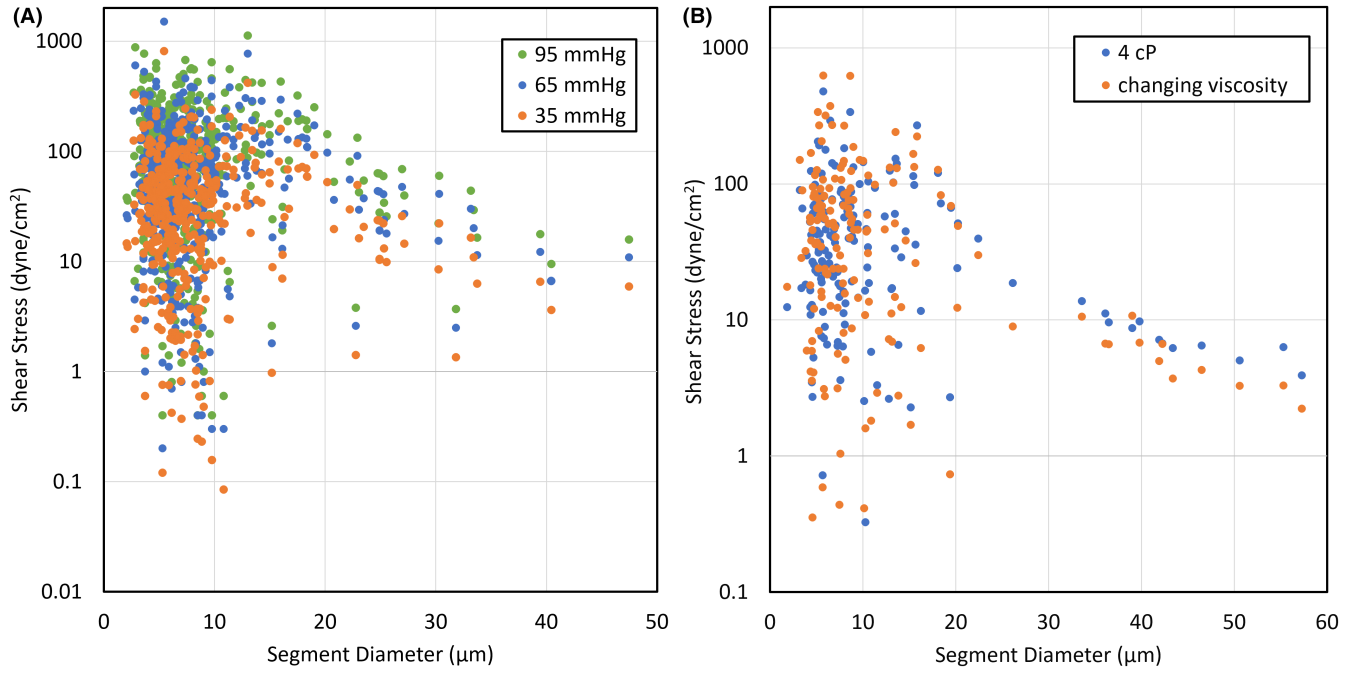

FIGURE 4 Shear stress estimates for a network with different pressure inputs and vessel specific viscosities. A sensitivity analysis was done with the parameters of (1) pressure drops between the arteriole inlet and venule outlet and (2) the constant or segment-specific viscosity (A) Estimates for simulations with pressures drops equal to 35, 65, and 95 mmHg. (B) Comparison of simulations assuming constant viscosity and changing viscosity based on an empirical relationship dependent on vessel diameter and hematocrit.

simulations (Figure 5A–D). The regions were selected to represent different characteristic regions within a network (i.e., high vessel density, branching off a larger venule, and capillary diameter). Results were also represented by shear stress color maps with two ranges: (1) 0 to >200 dyne/cm^2 (Figure 5E–H) and (2) 0 to >50 dyne/cm^2 (Figure 5I–L). The shear stress data used for each respective network is the same between the two color maps (e.g., Figure 5E has the same shear stress data as Figure 5I), and is presented in this manner to help visualize the vessel-specific variability and facilitate comparisons. For example, in comparing Figure 5E–I, or Figure 5F–J, the distribution of colors appears more scattered or non-uniform for the high-range color map (Figure 5E or Figure 5F), which provides a qualitative representation of the scale of the shear stress variability. Variations are also observed for the smaller range color map (Figure 5I or Figure 5J), although to a much lesser degree. These observations contrast with the respective behaviors in comparing Figure 5g,H or Figure 5H,I, where the higher variability manifests for the smaller-range color map (Figure 5K or Figure 5L). Altogether, these figures provide qualitative examples of different shear stress heterogeneity characteristics predicted for the networks. Since selected local regions capture multiple inlets and outlets, boundary pressures were assigned based on the relationship between estimated segmental pressures and diameters reported by Pries et al.[20] (Figure 5M). The shear stress distribution in four small regions ranged from 0.1 to 518.7 dyne/cm^2 (average = 61 ± 3.4 dyne/cm^2; Figure 5N). Similar spatial heterogeneity was also characteristic of an additional larger angiogenic microvascular region (3200 segments; 0.003 to 2328.1 dyne/cm^2; average = 39.8 ± 1.6 dyne/cm^2; Figure 6.)

3.2 | Angiogenic microvascular networks display increased average shear stress and heterogeneity compared to unstimulated networks

To evaluate whether vessels in remodeled microvascular networks post-angiogenic stimuli experience elevated shear stresses compared to vessels in unstimulated networks, shear stresses were compared across regions from both types of networks. Four unstimulated regions were compared to the three analyzed regions. Angiogenic remodeling was confirmed by an increase in the number of segments per region area and the total segment length per region area (Figure 7a–d). The average shear stress in the unstimulated regions was lower than that in the angiogenic regions (unstimulated = 20.5 ± 2.16 dyne/cm^2; angiogenic = 81.3 ± 3.5 dyne/cm^2; $p < .05$; Figure 7e).

3.3 | Three-dimensional simulation with RBCs also predicts vessel-specific shear stress heterogeneity

While the rationale for using the network modeling approach is supported by both its previous use in the literature and our overall goal to estimate vessel-specific shear stress ranges across intact microvascular regions, the lack of RBCs and three-dimensional geometric complexity raise questions about the physiological applicability of the approach. However, vessel-specific average wall shear stresses estimated with 3D RBC-resolved simulations importantly suggest a similar spatial heterogeneity (Figure 8). Here,

15498719, 2023, 8, Downloaded from https://onlinelibrary.wiley.com/doi/10.1111/micc.12830 by Nj Institute Of Technology, Wiley Online Library on [03/06/2024]. See the Terms and Conditions (https://onlinelibrary.wiley.com/terms-and-conditions) on Wiley Online Library for rules of use; OA articles are governed by the applicable Creative Commons License

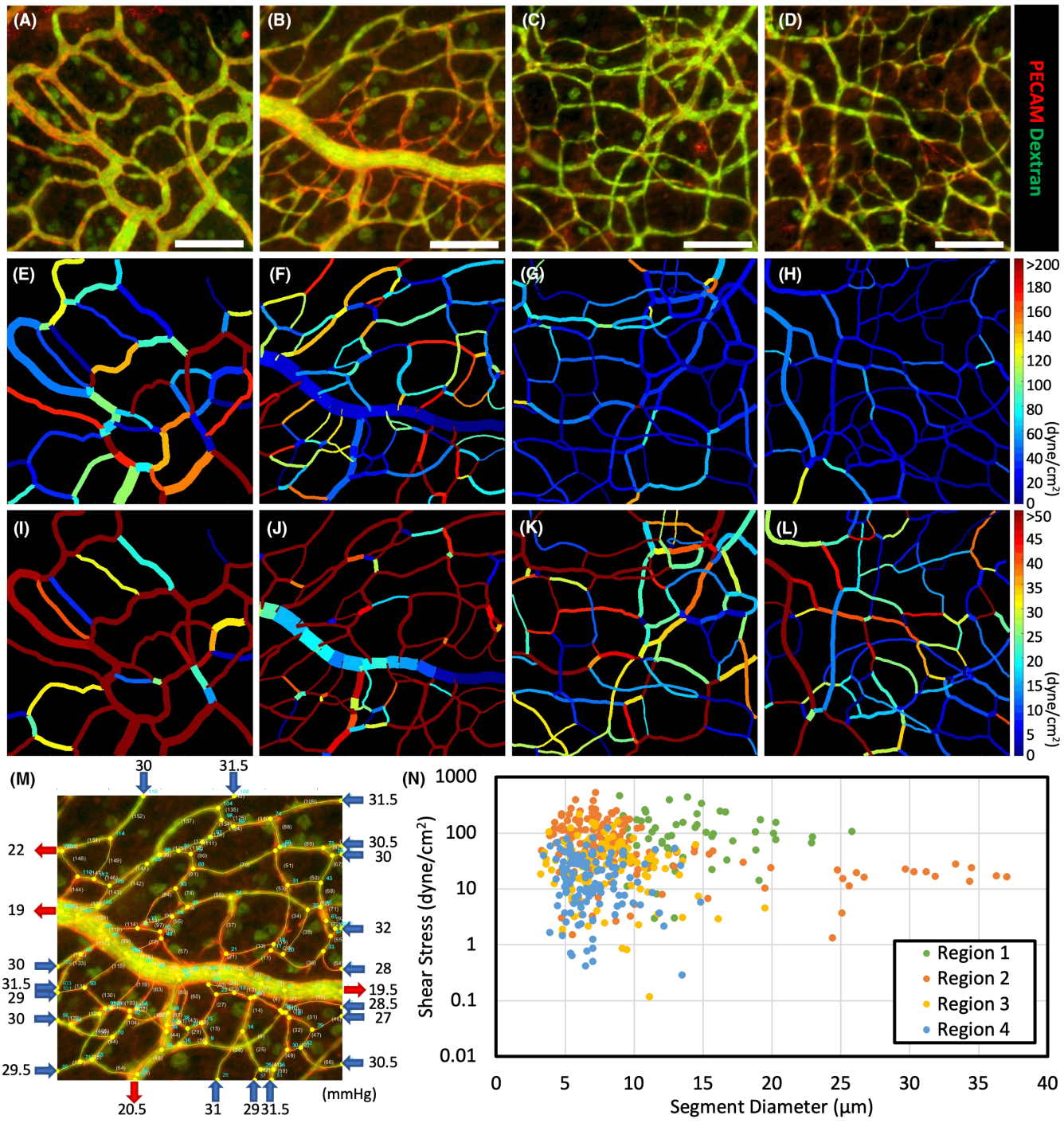

FIGURE 5 Shear stress estimates for single vascular segments in four vascular local regions. (A–D) Network local regions with complex vascular structures selected for simulations. Vessel walls labeled with PECAM were shown in red and vessels perfused with 40 kDa Dextran were shown in green. (E–H) Color maps of shear stress spatial distribution. Range = 0 (blue) to >200 (red) dyne/cm^2. (I–L) Color maps of shear stress spatial distribution. Range = 0 (blue) to >50 (red) dyne/cm^2. It is noted that the shear stress data used in (E)–(H) is the same as that used in (I–J), and the geometrical details of the networks (e.g., diameters) are the same between the two rows, respectively. Any apparent differences are likely due to visual artifacts arising from the same vessels being represented by different colors. (M) Illustration of assigning boundary pressures to vascular local regions (N) Distribution of shear stress values per segment diameter. Stress values in small segments (diameter: <10 μm) range from 0.1 to 518 dyne/cm^2.

due to the increased resolution, the concept of heterogeneity is further emphasized by (1) shear stress changes along complex surfaces of a vessel segment and (2) RBC-influenced time-dependent shear stress magnitudes and characteristics within individual vessels. For example, these representative simulations show shear stress spatial variations within a vessel can span on the order of 100 dyne/cm^2 at certain times and can fluctuate over time by as much as 350 dyne/cm^2. Yet, while the increased model resolution

15498719, 2023, 8, Downloaded from https://onlinelibrary.wiley.com/doi/10.1111/micc.12830 by Nj Institute Of Technology, Wiley Online Library on [03/06/2024]. See the Terms and Conditions (https://onlinelibrary.wiley.com/terms-and-conditions) on Wiley Online Library for rules of use; OA articles are governed by the applicable Creative Commons License

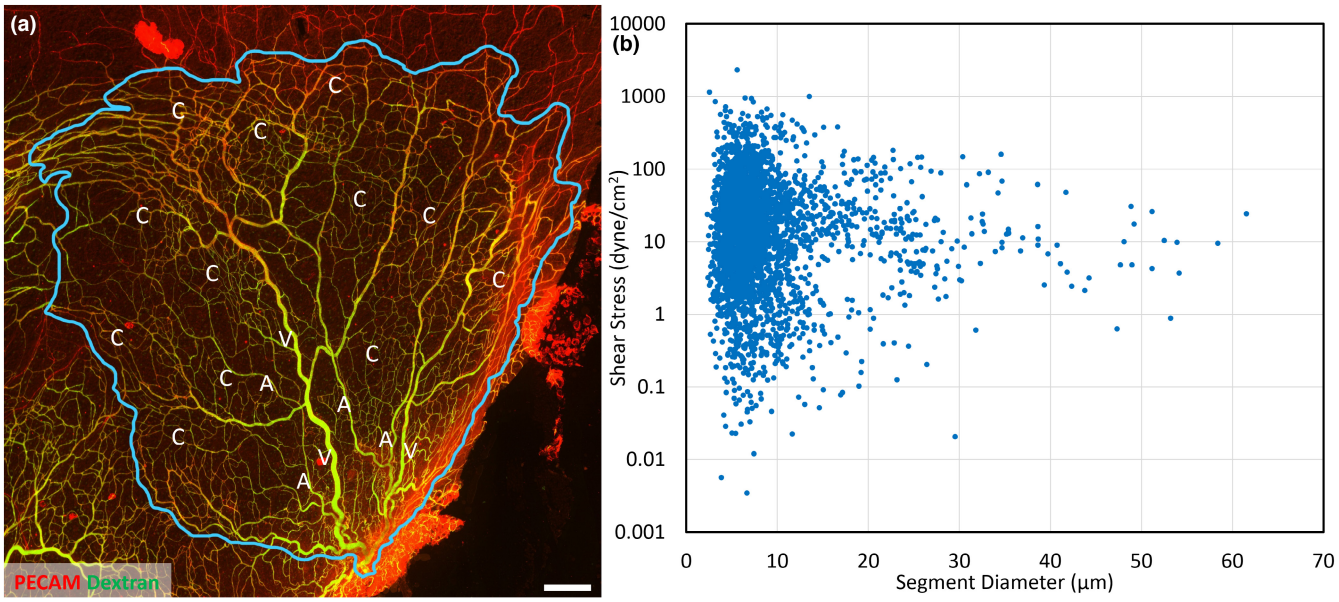

FIGURE 6 Shear stress estimates for single vascular segments in a vascular region montage. (a) Network region montage with angiogenic patterns selected for simulations. Vessel walls labeled with PECAM were shown in red and vessels perfused with 40 kDa Dextran were shown in green. (b) Distribution of shear stress values per segment diameter. Stress values in small segments (diameter: <10 μm) range from 0.1 to 2328 dyne/cm^2. Labels: A, arteriole, V, venule, C, capillaries. The blue line marks the selected vascular network regions for computational modeling.

FIGURE 7 Shear stress estimates for single vascular segments in unstimulated vascular regions. Representative images of network regions (a) unstimulated and (b) stimulated with 48–80 mast cell degranulation selected for simulations. Analysis was conducted to compare different metrics between unstimulated and stimulated vascular regions: (c) Segment density calculated by number of segments divided by vascular region area. (d) Segment length per area. (e) Estimated shear stress values, ranging from 0.1 to 528 dyne/cm^2 and 0.1 to 1114.3 dyne/cm^2 for unstimulated and stimulated regions. (Stimulated regions: $n = 3$, Unstimulated regions: $n = 4$) Labels: A, arteriole, V, venule, C, capillaries. The blue line marks the selected vascular network regions for computational modeling.

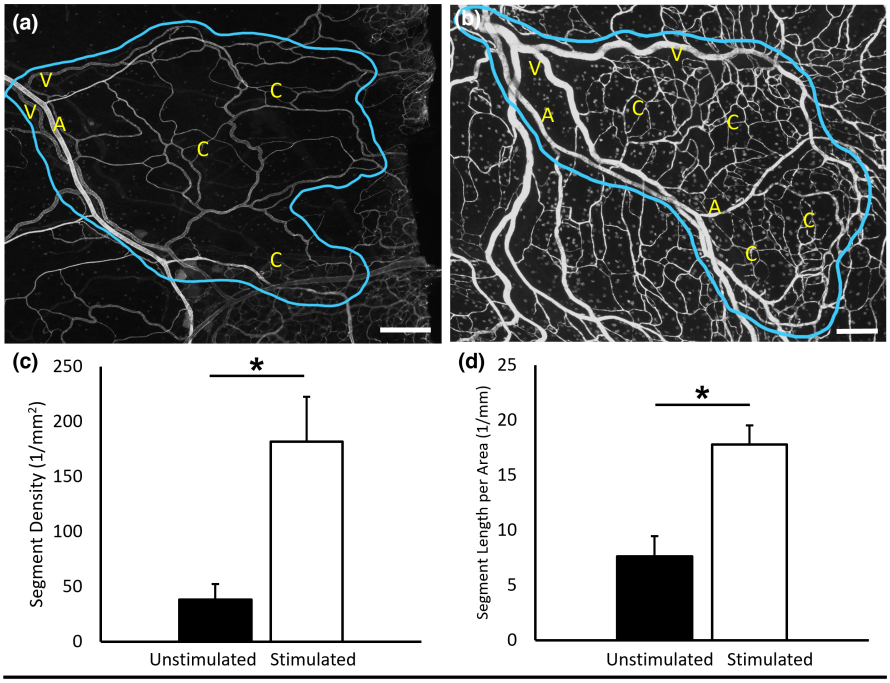

(e) Shear Stress (dyne/cm²)

	Average	Standard Deviation	Maximum	Minimum
Unstimulated	20.5	47.9	528.5	0.0009
Stimulated	81.3	103.2	1114.3	0.1

provides additional details, the degree of heterogeneity on a time-averaged per-vessel basis is similar to that predicted by the network approach.

To provide a comparison of predictions by the two different modeling approaches, the region in Figure 8 was also simulated using the network segment model. Shear stress statistics across

15498719, 2023, 8, Downloaded from https://onlinelibrary.wiley.com/doi/10.1111/micc.12830 by Nj Institute Of Technology, Wiley Online Library on [03/06/2024]. See the Terms and Conditions (https://onlinelibrary.wiley.com/terms-and-conditions) on Wiley Online Library for rules of use; OA articles are governed by the applicable Creative Commons License

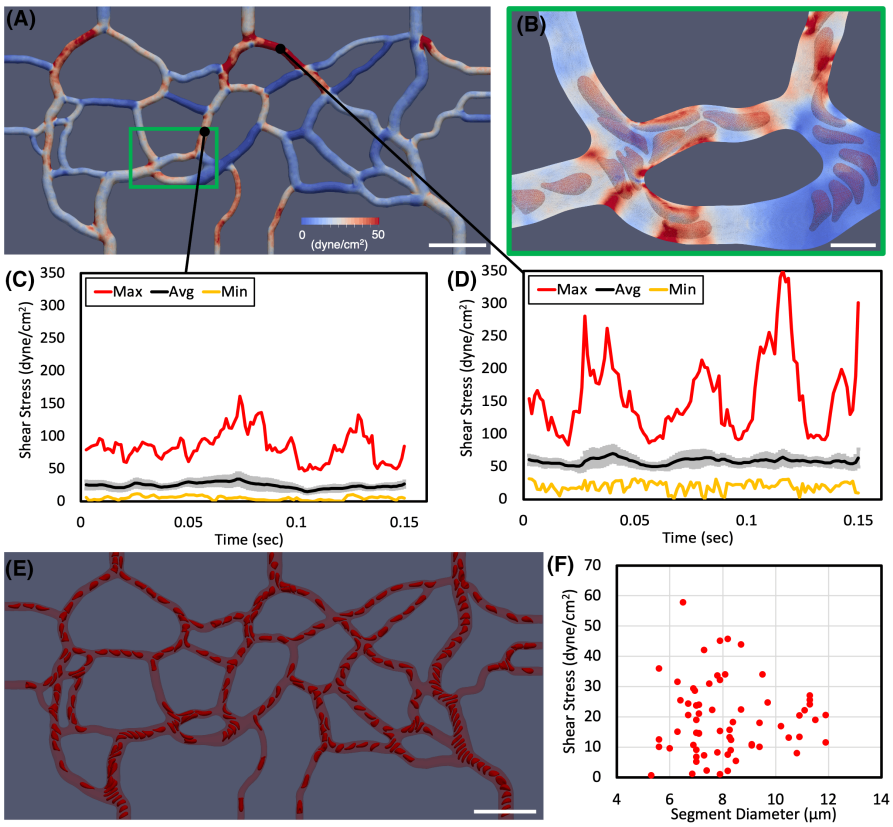

FIGURE 8 Wall shear stress estimates for vascular segments using a 3D model with RBCs. (A) Color map of shear stress spatial distribution. Range = 0 (blue) to 50 (red) dyne/cm^2. (B) A zoomed in view of color map of shear stress spatial distribution with RBCs illustrated. (C–D) Time-lapse shear stress estimates (Maximum, minimum, and average, with standard deviation shaded in grey) for two single vascular segments. (E) Snapshot of RBCs in the simulated angiogenic network region. (F) Distribution of time-averaged shear stress values per segment diameter. Stress values in small segments (diameter: <10 μm) range from 0.1 to 58 dyne/cm^2.

all network vessels for average, minimum, maximum, and standard deviation were 19.4 dyne/cm^2, 0.8 dyne/cm^2, 57.9 dyne/cm^2, and 12.1 dyne/cm^2 for the 3D model, and 18.1 dyne/cm^2, 0.02 dyne/cm^2, 61.0 dyne/cm^2, and 13.5 dyne/cm^2 for the network model. Overall, the general character of the shear stress distributions was similar, including the presence of vessel-specific heterogeneity. However, in comparing the two, it is important to consider that the vessel diameters used in the 3D model were generally not constant along the length, especially in connecting regions where morphologies are complex and 3D. Further, due to the small diameters and resulting RBC-scale effects and interactions with the geometry, the hemodynamic representation is fundamentally different.

4 | DISCUSSION

The main contribution of this study is the estimation of average shear stress values along microvessel segments in angiogenic networks. The range, vessel-specific heterogeneity, suggestion that vessel location is associated with a network, and effect of network patterns motivate new discussions regarding the actual shear stress values felt by endothelial cells and their association with angiogenic endothelial cell behavior. While many studies have established clear connections between wall shear stress and endothelial cell responses, our data and findings suggest that there are still a lot of open questions as to the actual microenvironment experienced by endothelial cells during angiogenesis. For example, what wall shear stresses are really experienced during angiogenesis? Just because in vitro studies have shown endothelial cells to respond to certain shear stress values, does this mean they experience such values in vivo? And because there is a significant range of in vitro values reported, how is one to know what might occur in a real angiogenic network? Based on the current literature, clear answers to such questions are lacking. The current study provides important direct estimates of shear stress values, variability, and distribution based on real angiogenic microvascular networks in the rat mesentery, in addition to comparisons with behavior in unstimulated networks from the same type of tissue, which show notable differences (Figure 7).

To understand what shear stress values were being associated with endothelial cell dynamics in the literature, we searched for "angiogenesis", "shear stress", and "endothelial cells" using PubMed and identified for approximately 100 studies the maximum shear stress used; most studies were in vitro. Interestingly, some studies stimulated cells with stresses as high as 100 dyne/cm^2, but greater than 90% of the studies used stresses less than 30 dyne/cm^2. Maybe more interestingly, about an equal amount of those studies used shear stresses distributed over the 0–30 dyne/cm^2 range (<10, 10–20, or >30 dyne/cm^2). The differential responses reported over the range of shear stresses and our findings emphasize the physiological importance of understanding how shear stresses vary from one vessel to another in a remodeling microvascular network and the implications of some local shear stresses being in excess of 1000 dyne/cm^2.

The heterogeneity of hemodynamic variables in the microcirculation has long been recognized[21,34] and has significant functional implications, for instance with regard to oxygen transport.[35] Such heterogeneity is inevitable as a consequence of known geometrical

15498719, 2023, 8, Downloaded from https://onlinelibrary.wiley.com/doi/10.1111/micc.12830 by Nj Institute Of Technology, Wiley Online Library on [03/06/2024]. See the Terms and Conditions (https://onlinelibrary.wiley.com/terms-and-conditions) on Wiley Online Library for rules of use; OA articles are governed by the applicable Creative Commons License

and developmental constraints on network structure, and compensatory mechanisms (structural adaptation and acute flow regulation) are needed to achieve adequate uniformity of perfusion throughout a tissue despite the underlying heterogeneity.[36] Responses to changes in wall shear stress are a key part of these compensatory mechanisms.[37,38] The present findings emphasize the significance of heterogeneity as a factor in the control of microvascular blood flow and suggest that investigations of the effects of wall shear stress on endothelial cells should examine wider stress ranges than have generally been considered in previous studies. Further, our results provoke the need to understand how the heterogeneous shear stresses might influence the roles of the other micro-environmental factors known to be involved in angiogenesis.

Our results also provide an example of the value of computational modeling approaches for making sense of microvascular physiology. While shear stresses can be estimated based on intravital measurements of local segmental velocities, the technical effort required to measure velocities in hundreds or thousands of vessels makes the approach a challenge. Compared to previous modeling studies, the current study offers shear stress estimates with intact angiogenic rat mesenteric networks, characterized by increased vessel density, sprouting, and apparent new segments from arterioles, venules, and capillaries. Our results, and specifically the segmental shear stress heterogeneity, are consistent with the reported shear stress estimates for unstimulated rat mesenteric networks using a similar modeling approach.[22] Our finding that shear stresses are increased in angiogenic versus unstimulated networks (Figure 7) along with the comparison of proximal versus distal vessels (Figure 3) further implicate the importance of angiogenic network patterns and vessel location. Increased shear stress along proximal capillaries compared to more distal regions is intuitive and provides a level of verification of the model. Further, this finding emphasizes the potential for specific network locations to be hot spots and highlights how, in a network, not every capillary is the same. The importance of vessel pattern is also realized when comparing our study to a computational study by Bernabeu et al. in which the authors reported lower shear stress variability at the capillary level in retinal networks.[26] Important notes are that capillaries in a retinal network predominately exist on the periphery of the network (i.e., after multiple branching from the arteriole side), and these capillaries likely experience different flow characteristics. Thus, the distribution of shear stresses can vary depending on network patterning, and the combined results of our study and the study by Bernabeu et al. motivate the evaluation of shear stresses for different tissues.

To our knowledge, no studies to-date have quantified distributions of average vessel wall shear stress values across angiogenic microvascular networks based on diameter and importantly, with comparisons to non-angiogenic networks from the same type of tissue. Distinguishing between angiogenic and non-angiogenic networks is important because microvascular network structures are known to be distinctly different. In the literature, many studies have reported shear stress values for non-angiogenic networks, including the aforementioned studies by Pries et al. from the rat mesentery[19–24] (0.1–500 dyne/cm^2 reported), work by Ganesan et. al. in murine retinal microvasculatures (0.1–300 dyne/cm^2 reported), and work by Frame and Sarelius[39] in cremaster muscle networks in hamsters (10–30 dyne/cm^2), to name a few. Such studies did report shear stress heterogeneity among vessels, with the most significant variations occurring in capillaries with diameters generally less than 10 μm. The latter of these studies[39] involved vessels with diameters greater than 10 μm, which is a possible reason for the reduced variability compared to the others. Nevertheless, the wall shear stress values and trends reported by such works are important to provide context for the current work in angiogenic microvascular networks and motivate the major questions addressed concerning the stress values and distributions that can occur across real angiogenic microvasculatures with comparison to behavior in unstimulated networks. For the current work, the increase observed in average shear stress in the angiogenic networks as compared to the non-angiogenic networks might, in part, be due to the same boundary conditions being applied to both scenarios. For the angiogenic networks, there are generally more flow paths due to increased vessel density, leading to less resistance and more flow. The exact causes of the shear stress increase, however, are difficult to discern without knowing the real local pressures and flows. Our results show that pattern differences in network structures could cause shear stress differences; however, future studies informed by such measurements are needed to determine more precise influences of network patterning unique to angiogenic structures.

As previously noted, existing studies involving wall shear stress predictions in angiogenic microvascular networks are extremely rare. The work by Bernabeou et al.[26] showed shear stress contours on vessels across developing retinal networks, with values shown up to 200 dyne/cm^2, although the average per-vessel values in relation to diameter were not directly reported. They also deemed values greater than 200 dyne/cm^2 as unphysiological because prior works cited (in unstimulated, non-angiogenic networks) did not report values this high. This further prompts the question, specifically with regard to angiogenesis, of what is physiological? Other work by Ghaffari et al.[40] predicted much lower shear stress values (up to 2 dyne/cm^2) in isolated microvascular loop structures in avian chick embryos. Given the scarcity of studies reporting shear stress values in real angiogenic microvasculatures, the findings reported here push an important scientific discussion. Notably, given the number of in vitro studies that implicate shear stress as a regulator of endothelial cell dynamics, our results emphasize the need for careful consideration of the shear stress stimuli values. For example, do differences in response to 5 dyne/cm^2 versus 10 dyne/cm^2 matter if the stresses range in a real network over an order of magnitude? And further, how do such ranges vary among different tissue types, organs, etc.? Such considerations, in conjunction with the current findings, warrant new discussions on the shear stress behaviors that actually occur during angiogenesis in vivo.

With regard to the interpretation of the current model results, an important consideration is the accuracy with which the networks were reconstructed from the imaging. More specifically, the measurements of vessel diameters for those less than roughly 5 μm may

15498719, 2023, 8, Downloaded from https://onlinelibrary.wiley.com/doi/10.1111/micc.12830 by Nj Institute Of Technology, Wiley Online Library on [03/06/2024]. See the Terms and Conditions (https://onlinelibrary.wiley.com/terms-and-conditions) on Wiley Online Library for rules of use; OA articles are governed by the applicable Creative Commons License

be subject to some degree of uncertainty given the small size and the optical resolution of the imaging. We note, however, that a main contribution of this work is the reported shear stress range and that this heterogeneity is consistent across our various networks with different diameters. Thus, the impact of the diameter measurements on our conclusions is expected to be small since the findings support a more dominant influence of network patterning than potential changes to vessel diameter due to measurement resolution. To test this, we performed several additional simulations in which capillary diameters less than 10 μm were altered in order to probe the sensitivity of our conclusions to diameter values in this range. Specifically, we adjusted these capillaries such that (i) each diameter was increased by 10%, (ii) each diameter was decreased by 10%, (iii) all capillaries have 10 μm diameters, and (iv) all capillaries have 5 μm diameters. For the baseline case, we observed a relative standard deviation of shear stress values (standard deviation divided by the mean) across all data points of 1.17, while values of 1.13, 1.13, 1.23, and 1.45 were observed for cases (i–iv), respectively. While the predicted wall shear stress values changed for the same vessels, the range of values and heterogeneity across the network were of similar magnitude. Full distributions of wall shear stress for each case are provided in the Data S1. This supports the impact of network patterning rather than changes to capillary diameters due to measurement resolution.

Assumptions related to inlet/outlet pressure boundary conditions, viscosity, and the lack of consideration for RBCs or vessel tortuosity warrant discussion. Regarding the pressure boundary conditions, we do not know the physiologically appropriate pressures for our angiogenic networks and used values consistent with previous studies.[20,22] We note that, given our 48/80 angiogenic stimulus and that prior work has shown this can induce hypotension in rats,[41] the potential for altered pressures at boundaries exists in such stimulated tissue. To address this, we ran simulations with different pressure boundary conditions (35, 65, 95 mm Hg). The range of shear stresses observed for the three cases was all very similar (Figure 4a) suggesting that the altered pressure differences are not sufficient to offset the shear stress distribution. Further, the sensitivity analysis (Figure 5) suggests that the main findings of spatial shear stress heterogeneity and variation across orders of magnitude are consistent with altered pressure conditions. So, while the actual shear stress values remain uncertain, we speculate that our results suggest a potential physiologically relevant range for the angiogenic tissues modeled here. These observations are not meant to suggest that the shear stress distribution is unaffected by driving pressures, but rather that these different conditions do not fundamentally alter the general character of the heterogeneity. Although beyond the current scope, a more in-depth sensitivity study is likely warranted to reveal specific mechanisms or causes for the higher shear stress values reported here versus prior works and to explore model limitations versus what actually occurs in vivo.

Regarding viscosity, our simulations assume a constant viscosity (4 cp). Allowing viscosity to change per segment dependent on empirically derived relationships between segmental flows, diameters, and hematocrit also did not alter the study's main findings (Figure 5). And because shear stress is proportional to segment diameter, pressure drop, and length, the constant viscosity value does not matter. Finally, physiological flows are not single-phase through segmental networks. The associated limitation of our modeling approach motivates future work to apply more complicated three-dimensional dynamic models that incorporate RBCs and 3D surface complexity, similar to our previous work.[25] A major benefit of the network segmental model approach, however, is the decreased computational cost compared to high-resolution 3D models. So, while more complicated dynamic models could potentially provide more physiologically relevant information, a critical question remains. What can we learn with our simpler approach? Based on an initial application of our 3D simulation approach for a "small" region (Figure 8), our network segmental analysis is sufficient to generally predict time-averaged shear stress spatial heterogeneity on a per-vessel basis. The results of the 3D simulation additionally emphasize the potential for temporal and spatial variations along specific segments and the impacts of RBCs.

Another potential limitation of our study is the use of rat mesentery tissues. As mentioned above, future studies will be needed to evaluate shear stresses in angiogenic networks from other tissues. The rat mesentery was used for this study because it is 20–40 μm thick, and its thinness makes it relatively easy to image with a standard epifluorescent microscope. Also, the mesentery provides branched microvascular networks and has been previously used for computational estimation of vessel specific hemodynamics.[22,42,43] Also, the 48–80 angiogenesis stimulation, which has been well characterized by our group and others,[28,44] results in robust angiogenic remolding across the hierarchy of networks. Future studies are also needed to evaluate shear stress distributions for alternative remodeling stimuli.

5 | PERSPECTIVES

The results of our current study suggest that shear stress magnitudes along microvessels in angiogenically remodeled networks vary over a wide range. An appreciation of this potential variation from one vessel to another adds a valuable perspective for understanding how local shear stresses trigger or regulate endothelial cell dynamics involved in capillary sprouting. The potential for heterogeneous local shear stress distributions is realized even more when we consider the influences of vessel shape and the flow of RBCs. The results motivate future studies that incorporate capillary sprout dynamics, including initial sprout formation, sprout extension, and sprout connection. Understanding the local shear stresses over the spatial and temporal time course of angiogenesis will further guide our understanding of the role of shear stress in regulating endothelial cell behavior.

AUTHOR CONTRIBUTIONS

Conceptualization: Walter L. Murfee, Peter Balogh. *Methodology*: Walter L. Murfee, Peter Balogh. *Investigation*: Nien-Wen Hu, MMN Hossain, Walter L. Murfee, Peter Balogh, Banks M. Lomel, Elijah W. Rice. *Visualization*: Nien-Wen Hu, Walter L. Murfee, Peter Balogh.

15498719, 2023, 8, Downloaded from https://onlinelibrary.wiley.com/doi/10.1111/micc.12830 by Nj Institute Of Technology, Wiley Online Library on [03/06/2024]. See the Terms and Conditions (https://onlinelibrary.wiley.com/terms-and-conditions) on Wiley Online Library for rules of use; OA articles are governed by the applicable Creative Commons License

Supervision: Walter L. Murfee, Peter Balogh, Timothy W. Secomb, Malisa Sarntinoranont. *Writing*: Nien-Wen Hu, Walter L. Murfee, Peter Balogh, Timothy W. Secomb.

ACKNOWLEDGMENTS

We would like to thank the members of the Murfee Microvascular Dynamics Laboratory at the University of Florida and members of the Microcirculatory Society for their valuable discussion of the results. Computational resources on the Lochness Compute Cluster at the New Jersey Institute of Technology are acknowledged for the 3D RBC-resolved simulations.

FUNDING INFORMATION

NIH grant R21HL159501. University of Florida Health Cancer Center Pilot Grant No. 00096885 CA-FY22-03.

CONFLICT OF INTEREST STATEMENT

The authors declare no conflicts of interest.

DATA AVAILABILITY STATEMENT

All data will be made available upon request.

ORCID

Mir Md Nasim Hossain https://orcid.org/0009-0000-1189-5100
Timothy W. Secomb https://orcid.org/0000-0002-0176-5502
Walter L. Murfee https://orcid.org/0000-0002-8247-4722
Peter Balogh https://orcid.org/0000-0002-1503-4305

REFERENCES

1. Murfee WL. Implications of fluid shear stress in capillary sprouting during adult microvascular network remodeling. *Mechanobiology of the Endothelium*; CRC Press. 2015:166.
2. Skalak TC, Price RJ. The role of mechanical stresses in microvascular remodeling. *Microcirculation*. 1996;3(2):143-165.
3. Galie PA, Nguyen DHT, Choi CK, Cohen DM, Janmey PA, Chen CS. Fluid shear stress threshold regulates angiogenic sprouting. *Proc Natl Acad Sci U S A*. 2014;111(22):7968-7973.
4. Kadohama T, Nishimura K, Hoshino Y, Sasajima T, Sumpio BE. Effects of different types of fluid shear stress on endothelial cell proliferation and survival. *J Cell Physiol*. 2007;212(1):244-251.
5. Yamamoto K, Takahashi T, Asahara T, et al. Proliferation, differentiation, and tube formation by endothelial progenitor cells in response to shear stress. *J Appl Physiol*. 2003;95(5):2081-2088.
6. Lamalice L, Le Boeuf F, Huot J. Endothelial cell migration during angiogenesis. *Circ Res*. 2007;100(6):782-794.
7. dela Paz NG, Walshe TE, Leach LL, Saint-Geniez M, D'Amore PA. Role of shear-stress-induced VEGF expression in endothelial cell survival. *J Cell Sci*. 2012;125(4):831-843.
8. Deng H, Min E, Baeyens N, et al. Activation of Smad2/3 signaling by low fluid shear stress mediates artery inward remodeling. *Proc Natl Acad Sci*. 2021;118(37):e2105339118.
9. Buchanan CF, Verbridge SS, Vlachos PP, Rylander MN. Flow shear stress regulates endothelial barrier function and expression of angiogenic factors in a 3D microfluidic tumor vascular model. *Cell Adh Migr*. 2014;8(5):517-524.
10. Topper JN, Gimbrone MA Jr. Blood flow and vascular gene expression: fluid shear stress as a modulator of endothelial phenotype. *Mol Med Today*. 1999;5(1):40-46.
11. Russo TA, Banuth AMM, Nader HB, Dreyfuss JL. Altered shear stress on endothelial cells leads to remodeling of extracellular matrix and induction of angiogenesis. *PLoS One*. 2020;15(11):e0241040.
12. Song JW, Munn LL. Fluid forces control endothelial sprouting. *Proc Natl Acad Sci*. 2011;108(37):15342-15347.
13. Kang H, Bayless KJ, Kaunas R. Fluid shear stress modulates endothelial cell invasion into three-dimensional collagen matrices. *Am J Physiol Heart Circ Physiol*. 2008;25(5):H2087-H2097.
14. Cullen JP, Sayeed S, Sawai RS, et al. Pulsatile flow–induced angiogenesis: role of G(i) subunits. *Arterioscler Thromb Vasc Biol*. 2002;22(10):1610-1616.
15. Deb N, Ali MS, Mathews A, Chang YW, Lacerda CM. Shear type and magnitude affect aortic valve endothelial cell morphology, orientation, and differentiation. *Exp Biol Med*. 2021;246(21):2278-2289.
16. Ye M, Sanchez HM, Hultz M, et al. Brain microvascular endothelial cells resist elongation due to curvature and shear stress. *Sci Rep*. 2014;4(1):1-6.
17. Schnittler HJ, Schneider SW, Raifer H, et al. Role of Actin filaments in endothelial cell-cell adhesion and membrane stability under fluid shear stress. *Pflugers Arch*. 2001;442(5):675-687.
18. Ganesan P, He S, Xu H. Analysis of retinal circulation using an image-based network model of retinal vasculature. *Microvasc Res*. 2010;80(1):99-109.
19. Pries AR, Secomb TW, Gessner T, Sperandio MB, Gross JF, Gaehtgens P. Resistance to blood flow in microvessels in vivo. *Circ Res*. 1994;75(5):904-915.
20. Pries AR, Secomb TW, Gaehtgens P. Design principles of vascular beds. *Circ Res*. 1995a;77(5):1017-1023.
21. Pries AR, Secomb TW, Gaehtgens P. Structure and hemodynamics of microvascular networks: heterogeneity and correlations. *Am J Physiol Heart Circ Physiol*. 1995b;269(5):H1713-H1722.
22. Pries AR, Secomb TW, Gaehtgens P. Structural adaptation and stability of microvascular networks: theory and simulations. *Am J Physiol Heart Circ Physiol*. 1998;275(2):H349-H360.
23. Pries AR, Reglin B, Secomb TW. Structural adaptation of microvascular networks: functional roles of adaptive responses. *Am J Physiol Heart Circ Physiol*. 2001;281(3):H1015-H1025.
24. Pries AR, Reglin B, Secomb TW. Structural response of microcirculatory networks to changes in demand: information transfer by shear stress. *Am J Physiol Heart Circ Physiol*. 2003;284(6):H2204-H2212.
25. Balogh P, Bagchi P. Three-dimensional distribution of wall shear stress and its gradient in red cell-resolved computational modeling of blood flow in in vivo-like microvascular networks. *Physiol Rep*. 2019;7(9):14067.
26. Bernabeu MO, Jones ML, Nielsen JH, et al. Computer simulations reveal complex distribution of haemodynamic forces in a mouse retina model of angiogenesis. *J R Soc Interface*. 2014;11(99):20140543.
27. Hudetz AG, Greene AS, Fehér G, Knuese DE, Cowley AW Jr. Imaging system for three-dimensional mapping of cerebrocortical capillary networks in vivo. *Microvasc Res*. 1993;46(3):293-309.
28. Sweat RS, Stapor PC, Murfee WL. Relationships between lymphangiogenesis and angiogenesis during inflammation in rat mesentery microvascular networks. *Lymphat Res Biol*. 2012;10(4):198-207.
29. Yang M, Murfee WL. The effect of microvascular pattern alterations on network resistance in spontaneously hypertensive rats. *Med Biol Eng Comput*. 2012;50(6):585-593.
30. Pries AR, Secomb TW, Gaehtgens P, Gross JF. Blood flow in microvascular networks. Experiments and simulation. *Circ Res*. 1990;67(4):826-834.
31. Balogh P, Bagchi PA. Computational approach to modeling cellular-scale blood flow in complex geometry. *J Comput Phys*. 2017;334:280-307.
32. Skalak R, Tozeren A, Zarda RP, Chien S. Strain energy function of red blood cell membranes. *Biophys J*. 1973;13(3):245-264.

15498719, 2023, 8, Downloaded from https://onlinelibrary.wiley.com/doi/10.1111/micc.12830 by Nj Institute Of Technology, Wiley Online Library on [03/06/2024]. See the Terms and Conditions (https://onlinelibrary.wiley.com/terms-and-conditions) on Wiley Online Library for rules of use; OA articles are governed by the applicable Creative Commons License

33. Mohandas N, Evans E. Mechanical properties of the red cell membrane in relation to molecular structure and genetic defects. *Annu Rev Biophys Biomol Struct*. 1994;23(1):787-818.
34. Zweifach BW. Quantitative studies of microcirculatory structure and function: I. analysis of pressure distribution in the terminal vascular bed in cat mesentery. *Circ Res*. 1974;34(6):841-857.
35. Roy TK, Secomb TW. Functional implications of microvascular heterogeneity for oxygen uptake and utilization. *Physiol Rep*. 2022;10(10):e15303.
36. Pries AR, Secomb TW. Origins of heterogeneity in tissue perfusion and metabolism. *Cardiovasc Res*. 2009;81(2):328-335.
37. Kuo L, Davis MJ, Chilian WM. Endothelium-dependent, flow-induced dilation of isolated coronary arterioles. *Am J Physiol Heart Circ Physiol*. 1990;259(4):H1063-H1070.
38. Rodbard S. Vascular caliber. *Cardiology*. 1975;60(1):4-49.
39. Frame MD, Sarelius IH. Endothelial cell dilatory pathways link flow and wall shear stress in an intact arteriolar network. *J Appl Physiol*. 1996;81(5):2105-2114.
40. Ghaffari S, Leask RL, Jones EA. Flow dynamics control the location of sprouting and direct elongation during developmental angiogenesis. *Development*. 2015;142:4151-4157.
41. Hannon JP, Pfannkuche HJ, Fozard JR. A role for mast cells in adenosine A3 receptor-mediated hypotension in the rat. *Br J Pharmacol*. 1995;115(6):945-952.
42. Hu NW, Rodriguez CD, Rey JA, et al. Estimation of shear stress values along endothelial tip cells past the lumen of capillary sprouts. *Microvasc Res*. 2022;142:104360.
43. Stapor PC, Wang W, Murfee WL, Khismatullin DB. The distribution of fluid shear stresses in capillary sprouts. *Cardiovasc Eng Tech*. 2011;2(2):124-136.
44. Norrby K, Jakobsson A, Sörbo J. Mast-cell-mediated angiogenesis: a novel experimental model using the rat mesentery. *Virchows Archiv B*. 1986;52:195-206.

SUPPORTING INFORMATION

Additional supporting information can be found online in the Supporting Information section at the end of this article.

How to cite this article: Hu N-W, Lomel BM, Rice EW, et al. Estimation of shear stress heterogeneity along capillary segments in angiogenic rat mesenteric microvascular networks. *Microcirculation*. 2023;30:e12830. doi:10.1111/micc.12830

15498719, 2023, 8, Downloaded from https://onlinelibrary.wiley.com/doi/10.1111/micc.12830 by Nj Institute Of Technology, Wiley Online Library on [03/06/2024]. See the Terms and Conditions (https://onlinelibrary.wiley.com/terms-and-conditions) on Wiley Online Library for rules of use; OA articles are governed by the applicable Creative Commons License